

# Bioactive $\text{Ag}_3\text{PO}_4$ /Polypropylene Composites for Inactivation of SARS-CoV-2 and Other Important Public Health Pathogens

Lara K. Ribeiro, Marcelo Assis,\* Lais R. Lima, Dyovani Coelho, Mariana O. Gonçalves, Robert S. Paiva, Leonardo N. Moraes, Lauana F. Almeida, Felipe Lipsky, Miguel A. San-Miguel, Lúcia H. Mascaro, Rejane M. T. Grotto, Cristina P. Sousa, Ieda L. V. Rosa, Sandra A. Cruz, Juan Andrés, and Elson Longo



Cite This: *J. Phys. Chem. B* 2021, 125, 10866–10875



Read Online

ACCESS |



Metrics & More

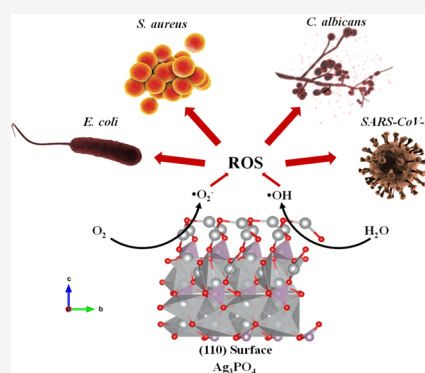


Article Recommendations



Supporting Information

**ABSTRACT:** The current unprecedented coronavirus pandemic (COVID-19) is increasingly demanding advanced materials and new technologies to protect us and inactivate SARS-CoV-2. In this research work, we report the manufacture of  $\text{Ag}_3\text{PO}_4$  (AP)/polypropylene (PP) composites using a simple method and also reveal their long-term anti-SARS-CoV-2 activity. This composite shows superior antibacterial (against *Staphylococcus aureus* and *Escherichia coli*) and antifungal activity (against *Candida albicans*), thus having potential for a variety of technological applications. The as-manufactured materials were characterized by XRD, Raman spectroscopy, FTIR spectroscopy, AFM, UV–vis spectroscopy, rheology, SEM, and contact angle to confirm their structural integrity. Based on the results of first-principles calculations at the density functional level, a plausible reaction mechanism for the initial events associated with the generation of both hydroxyl radical  $\cdot\text{OH}$  and superoxide radical anion  $\cdot\text{O}_2^-$  in the most reactive (110) surface of AP was proposed. AP/PP composites proved to be an attractive avenue to provide human beings with a broad spectrum of biocide activity.



## 1. INTRODUCTION

Currently, human beings have been facing a critical problem with the pandemic caused by the emergence of the SARS-CoV-2 virus.<sup>1–3</sup> Microorganisms (including bacteria, fungi, and viruses) pose serious threats to public health. Particularly, viruses are one of the main causes of diseases worldwide, being responsible for infecting and killing a large part of the population in a given area.<sup>4,5</sup> Coronaviruses, a class of viruses, are constituted of positive single-stranded RNAs and belong to the *Coronaviridae* family.<sup>6</sup> The establishment of viral tropism depends on the susceptibility and permissiveness of a particular host cell. These types of viruses usually infect animals and humans due to their incredible ability to adapt to their current host, causing respiratory problems and some flu-like symptoms.<sup>6–8</sup>

SARS-CoV-2 is transmitted by human body fluids and the virion can gain entry through nasopharyngeal and/or oropharyngeal tissues.<sup>9–13</sup> Recent studies have reported that these viruses can survive for several days on different surfaces.<sup>14–16</sup> In view of this scenario, efforts in research, development, and manufacture of materials with anti-SARS-CoV-2 activity are increasing, generating potentially safe alternatives to prevent virus contamination and transmission in humans.<sup>17</sup>

Innovations often play an essential role in the acceleration of the discovery of new functional materials.<sup>18</sup> However, their success and applicability largely depend on previous experi-

ence. Our research group has been developing potent biocide materials based on complex silver-based oxides, such as  $\text{Ag}_2\text{CrO}_4$ ,<sup>19,20</sup> three polymorphs of  $\text{Ag}_2\text{WO}_4$ ,<sup>21,22</sup>  $\text{Ag}_3\text{PO}_4$ ,<sup>23,24</sup>  $\alpha\text{-AgVO}_3$ ,<sup>25</sup> and  $\beta\text{-Ag}_2\text{MoO}_4$ <sup>26</sup> with enhanced antifungal activity. Additionally, to provide a deeper understanding of the atomic and electronic structure and to establish a correlation between the morphology and the biocide activity, we conducted first-principles calculations at the DFT level to complement and rationalize the experimental findings.<sup>27</sup>

Silver orthophosphate,  $\text{Ag}_3\text{PO}_4$  (AP), is an n-type semiconductor with a band gap energy value of 2.4 eV, having high quantum efficiency until 90% for  $\text{O}_2$  evolution from  $\text{H}_2\text{O}$  splitting.<sup>28–34</sup> Despite its high photocatalytic activities, notable drawbacks have emerged in relation to this material, that is, it invariably displays poor stability when forming metallic  $\text{Ag}^{35–39}$  or dissolved in water,<sup>40</sup> possibly leading to partial dissociation of AP into  $\text{Ag}^+$  and  $\text{PO}_4^{3-}$ .<sup>41</sup> All of these drawbacks have weakened its activity, thus reducing its broad application as a biocide agent. Very recently, Li et al.<sup>42</sup> discussed and summarized the progress to improve its stability

Received: June 14, 2021

Revised: September 8, 2021

Published: September 21, 2021



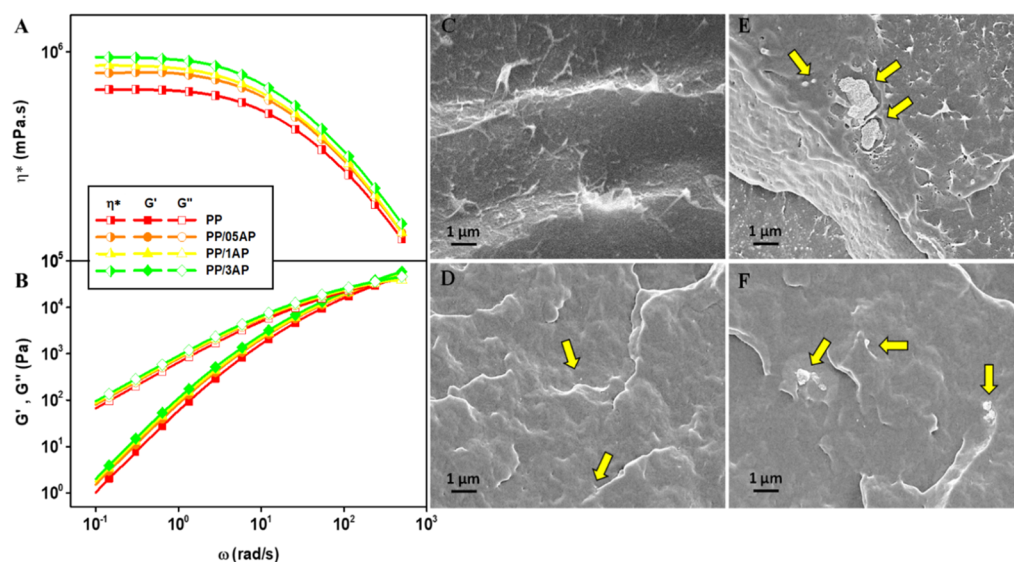


**Figure 1.** (A) Complex viscosity as a function of frequency; (B) storage modulus ( $G'$ ) and loss modulus ( $G''$ ) of the samples; and cross-sectional SEM images of (C) PP, (D) PP/0.5AP, (E) PP/1AP, and (F) PP/3AP.

and performance, as well as the barriers that should be overcome prior to practical application.

Polypropylene (PP) is a chemically and thermally stable polymer with a wide range of applications, from textile to automotive industries, and one of the most used plastics worldwide since the mid-20th century.<sup>43</sup> PP is used as an immobilization matrix and a substrate for biocompatibility and biocide activity tests in devices of the hospital-medical field, such as masks, aprons, and food trays, among other applications.<sup>44,45</sup> Based on that, the strategy adopted in this work was to produce a bioactive AP/PP composite to stabilize AP, and the inactivation of bacteria (*Staphylococcus aureus* and *Escherichia coli*), fungus (*Candida albicans*), and virus (SARS-CoV-2) has been investigated. The present composites have the potential for a variety of technological applications, such as the manufacture of packaging, fabrics, and protective equipment, as well as for surface treatment. The underlying technology based on this composite can be considered as an innovation to protect man and avoid the contamination, transmission, and proliferation of SARS-CoV-2 worldwide.

## 2. METHODS

**Synthesis of AP.** AP was synthesized by the coprecipitation method in aqueous medium. Separate solutions of  $\text{NaH}_2\text{PO}_4 \cdot \text{H}_2\text{O}$  (98%, Sigma-Aldrich) and  $\text{AgNO}_3$  (99.8%, Cennabras) were prepared with molar ratios of 1:1. The 100 mL solution of  $1 \times 10^{-3}$  mol of  $\text{NaH}_2\text{PO}_4$  was added to the 100 mL solution of  $1 \times 10^{-3}$  mol of  $\text{AgNO}_3$  under constant stirring. After the addition, the suspension was stirred for 20 min. The precipitates were washed with deionized water and centrifuged, and this process was repeated until pH neutrality ( $\cong 7$ ) was reached. After the washing procedure, this powder was dried at 60 °C for 10 h. The samples were labeled as AP.

**Preparation of PP/AP Composites.** The composites were compounded using an internal mixer (Thermo Scientific—Polylab OS model) with a counter-rotating rotor connected to the Rheomix 600 OS Lab mixing chamber. The conditions employed within the closed and locked chamber were a temperature of 200 °C and a rotor speed of 50 rpm for 4 min, which operated with 70% of its capacity. AP was added

to the polymer (PP) in proportions of 0.5, 1.0, and 3.0% wt. The processing conditions, especially those concerning the thread profile and temperatures, were outlined to ensure an adequate dispersive and distributive mixture. The samples were named according to the AP content as follows: PP/0.5AP, PP/1AP, and PP/3AP. The experimental characterizations, biological tests, and theoretical calculations are described in [Supporting Information](#) (Figures S1–S3).

## 3. RESULTS AND DISCUSSION

From the XRD patterns of the PP/AP composites, it is possible to observe that the alpha structure of PP was maintained, as well as the structure of the crystals of AP, suggesting the successful formation of the PP/AP composites (see Figure S4 in [Supporting Information](#)). These results corroborate with FTIR spectroscopy, micro-Raman, UV–vis, and atomic force microscopy (AFM) analyses, showing that at long and short ranges, the structure of AP is maintained within the polymeric matrix (Figures S5–S8). The interactions between the matrix and the AP particles, as well as their dispersion state, were evaluated by rheological measurements in the dynamic state, and SEM was conducted on cryogenically fractured samples (see Figure 1).

PP presents a pseudoplastic flow behavior with viscosity decrease as a function of frequency. A gradual increase in the viscosity of the Newtonian plateau region can be observed with the increase of the filler content. The low-frequency region named terminal zone is in the  $G' \propto \omega$  and  $G'' \propto \omega^2$  regions. When the degree of dispersion increases, powers 1 and 2 change to lower values.<sup>46</sup> Figure 1B presents the same inclination values, which means low dispersion exists between the filler and the polymer matrix because a percolation network was not observed. These results are in accordance with the SEM images (Figure 1C–F). The micrograph shown in Figure 1C shows the cross section of the nanocomposites, where it is possible to observe that pristine PP is a homogeneous material. As AP is added, it is possible to see the presence of spherical particles in the nanocomposites. A better dispersion is noticed for the PP/0.5AP sample (Figure 1D). As the concentration of AP increases for PP/1AP and

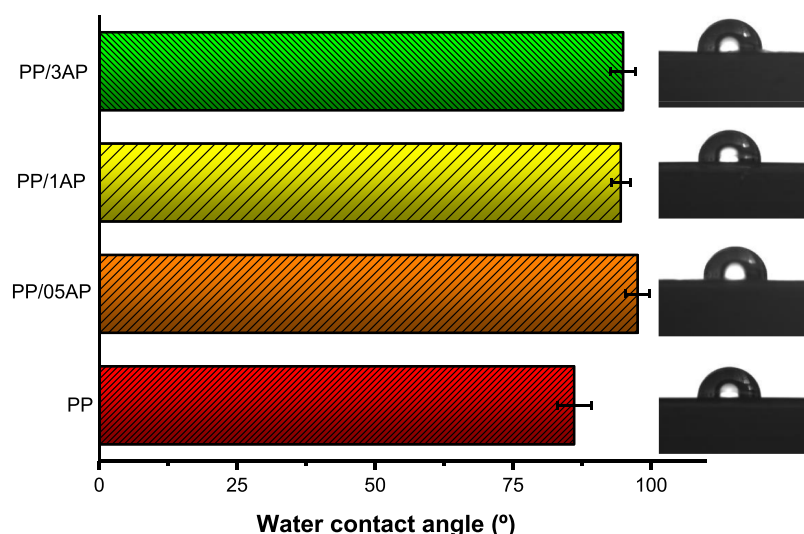


**Figure 2.** Contact angle results of pristine PP, PP/05AP, PP/1AP, and PP/3AP.

PP/3AP samples (Figure 1E,F), some micron-sized agglomerates of AP are formed, corroborating the structural data.

Figure 2 displays the contact angle results of the pristine PP and PP/AP composites. It is observed that for the PP sample, the contact angle value is  $86^\circ$  and it significantly increases to 98, 94, and  $95^\circ$  for the PP/05AP, PP/1AP, and PP/3AP samples, showing statistically significant differences between samples ( $p < 0.05$ ). Because PP is an apolar polymer with hydrophobic properties,<sup>47</sup> by increasing the AP semiconductor content, there is a consequent increase in hydrophobicity. Kasraei and Azarsina<sup>48</sup> observed the same behavior in Ag-based nanocomposites in polymeric matrices. The formation of a composite with a more hydrophobic surface may inhibit and/or decrease the activities of pathogenic microorganisms as a result of the lower interaction between the composite surface and the microorganism.<sup>49,50</sup>

Once AP was successfully incorporated into the polymeric PP matrix, contact microbicidal inhibition tests were performed for *S. aureus* (Gram +), *E. coli* (Gram -), and *C. albicans* (fungi). The time-kill tests (Figure 3) were carried out following the microbicidal evolution of the obtained materials to corroborate the halo of inhibition tests (Figure S9). The analyses were performed using time variations [2, 4, 8, 16, 32, 64, 128, 256, 512, 1440 (1 day), 2880 (2 days), and 4320 min (3 days)]. For *S. aureus* (Figure 3A), it was possible to note a reduction of 99.999% in colony-forming units (CFU) at the maximum time (3 days) for the PP/3AP sample. In contrast, for *E. coli* (Figure 3B), there was a reduction of 99.999% at 256 min ( $\sim 4.5$  h) for all composites. This difference between the elimination capacities of these tested bacteria was due to the fact that the composition of their membranes is very different, conferring greater resistance to the Gram + *S. aureus*.<sup>51–58</sup> For the elimination of *C. albicans*, that is, a more complex cellular constitution, the PP/3AP composite had contact elimination of 99% at the maximum time (3 days). For all microorganisms, it is observed that the PP/3AP sample was more effective, inactivating at least 99% of all microorganisms (bacteria and fungus) tested.

Concerning the elimination of more complex microorganisms, tests were carried out to verify the elimination of the SARS-CoV-2 virus by placing it on the surface of contact with the composite materials obtained for 5 min (see Figure 4). The

result of viricidal efficacy is negative when the cytopathic effects are visualized and positive when there is no cytopathic effect detected. To determine the viral inhibition index, the logarithmic difference between the control group and the group in contact with the composite samples (percentage of viral elimination compared to viral control, viral solution, and DMEN) was calculated. An analysis of the results renders that the PP and PP/05 AP samples (Figure 4A,B) do not show viral elimination, whereas the PP/1AP and PP/3AP samples (Figure 4C,D) reveal 90% viral elimination. The results regarding the increasing elimination as a function of the increase in the concentration of AP in PP are consistent with the detections expected because the microbicidal action comes from the semiconductor.<sup>59–64</sup> In addition, the semiconductor/polymer interaction impairs the surface fixation of pathogens in the composite, according to the contact angle results.

It is well established that the photocatalytic and biocide activities of a given semiconductor are dependent on the efficient formation and separation of electrons ( $e^-$ ) and holes ( $h^+$ ) and the low recombination ratio of the  $e^- - h^+$  pair. It has potent antimicrobial activity, which is typically associated with the contact-induced membrane stress and is associated with the presence of reactive oxygen species (ROS), thus having potential for a variety of biomedical applications.<sup>17,65–68</sup>

The activation of both molecular oxygen,  $O_2$ , and water,  $H_2O$ , is a fundamental step in almost all photocatalytic oxidation/reduction reactions and then the generation of ROS. At this point, it is important to note that the possible mechanism of the biocide activity is very dependent not only on the oxidation/reduction capacity of the different ROS but also on the nature of the radical chain reactions. Located in the valence band of the semiconductor,  $h^+$  reacts with  $H_2O$  to form a hydroxyl radical ( $\cdot OH$ ) and a proton ( $H^+$ ), while the  $e^-$ , which is excited in the conduction band, interacts with  $O_2$  to form  $\cdot O_2^-$ . Parallel reactions involving the formation of hydrogen peroxide ( $H_2O_2$ ), which is developed during the disproportionation of  $\cdot O_2^-$ , can also occur, further transforming it into  $\cdot OH$  and forming singlet oxygen ( $^1O_2$ ). In summary,  $\cdot OH$ ,  $H_2O_2$ ,  $\cdot O_2^-$ , and  $^1O_2$  are generated by the stepwise oxidation of  $H_2O$ , while the stepwise reduction of  $O_2$  generates  $\cdot O_2^-$ ,  $H_2O_2$ , and  $\cdot OH$ . These free radicals and reactive species are capable of killing microorganisms by the

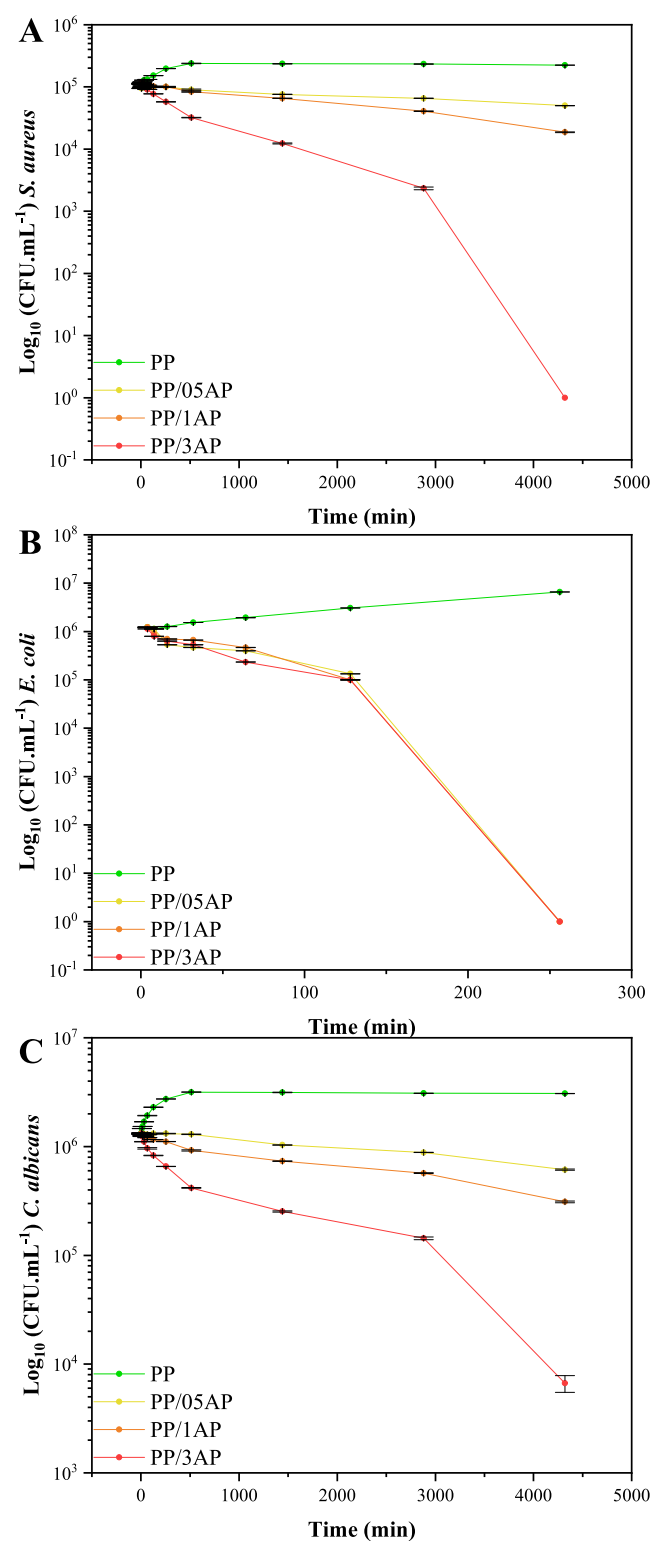


**Figure 3.** Time-kill curves of (A) *S. aureus*, (B) *E. coli*, and (C) *C. albicans* using PP, PP/05AP, PP/1AP, and PP/3AP samples.

oxidation and breaking of cellular constituents and membranes of bacteria, fungi, and viruses.<sup>69–74</sup> The ability to generate ROS has been explored by analyzing the adsorption processes of H<sub>2</sub>O and O<sub>2</sub> molecules on the AP (110) surface. This surface has been selected because several experimental<sup>75–79</sup> and theoretical studies<sup>80</sup> report that this surface is responsible for the high catalytic activity of AP.

The Ag cations on the first two layers of the clean (110) surface are low twofold coordinated in comparison with fourfold coordinated Ag cations in the bulk (see Figure 5A). This low coordination has already been reported as having a direct correspondence with increased biocide activity, consequently activating molecules that interact with an n-type semiconductor.<sup>81–83</sup> Bader analysis of the electron density distribution<sup>84</sup> reveals that these Ag cations are more reduced than the innermost ones. Thus, the effective charge of the AP (110) surface from the topmost layer is +0.50–0.52 |e|, whereas those of the Ag bulk cations are +0.41–0.44 |e|. This fact suggests that Ag superficial cations would be preferential sites for molecular adsorption, promoting electron transfer processes to account for their lack of electron density.

Different superficial Ag cations were considered as potential sites for the H<sub>2</sub>O molecule adsorption. The most favorable site with a calculated adsorption energy of –1.410 eV is depicted in Figure 5B. This adsorption process also distorts the surface with concomitant breaking bond processes between the Ag cation and the farthest O anion. The analysis of the bond critical points demonstrates a significant weakening of the covalent bond between the O atom of H<sub>2</sub>O and the H atom closer to the surface with concomitant enlargement of the bond distance from 0.97 to 1.10 Å. It is also shown that the H<sub>2</sub>O molecule establishes a second bond with the surface in the form of a weak covalent bond between its H atom and the nearest surface O atom. The emerging Ag–O interaction between the H<sub>2</sub>O molecule and the surface is characterized as van der Waals-type according to the Bader analysis. These results demonstrate that the n-type semiconductor surface activates the H<sub>2</sub>O molecule, leading to the formation of the •OH and H<sup>+</sup> species.

Ab initio molecular dynamics (AIMD) simulations at low temperatures (see Videos S1 and S2 in Supporting Information) starting from the described adsorption arrangement reveal the spontaneous breakage of the weakened O–H bond of the adsorbed H<sub>2</sub>O molecule, corresponding to the early events associated to the formation of •OH and H<sup>+</sup>, which remain adsorbed on the surface. There is a O–H bond involving the nearest O atom on the second layer, whereas the •OH is linked to the Ag cation on the first layer. At a higher temperature (50 K), this process occurs more rapidly, with more intense vibrational frequencies of both newly formed H–O and Ag–O bonds (Figure 5).

Similarly, an O<sub>2</sub> molecule is adsorbed on the surface at the same site with a calculated adsorption energy of –1.458 eV, as shown in Figure 6A. After the relaxation process, the molecule displays an increased bond length from 1.23 Å (for the free molecule) to 1.30 Å, a clear indication of bond weakening caused by the interaction with the surface (Figure 6B). Furthermore, the total spin calculated after adsorption corresponds to doublet oxygen (*S* = 1/2), differently from the triplet (*S* = 1) for the free O<sub>2</sub> molecule. These results can be associated with the initial events resulting from the formation of •O<sub>2</sub><sup>–</sup> in the AP (110) surface.

#### 4. CONCLUSIONS

Pathogenic microorganisms (bacteria, fungi, and viruses) represent a severe problem in public health. Therefore, there is great interest in developing advanced materials and new technologies capable of inactivating opportunistic pathogens, thus reducing the risk of infection and transmission. In this

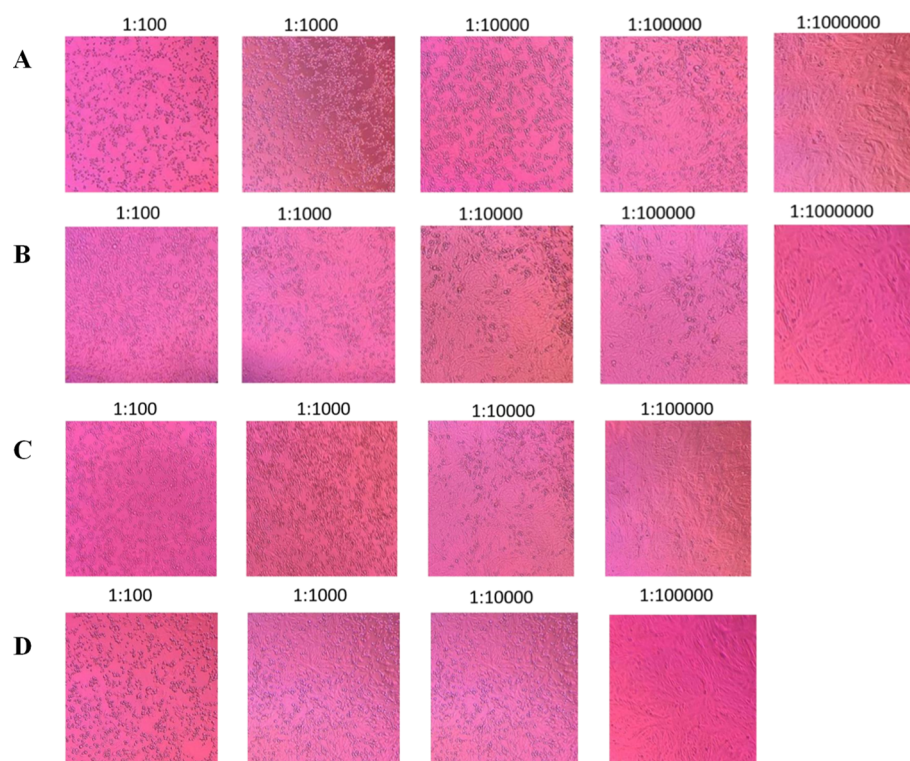


**Figure 4.** Microscopic images of cell cultures incubated with viral dilutions in contact with (A) PP, (B) PP/0.5AP, (C) PP/1AP, and (D) PP/3AP samples.

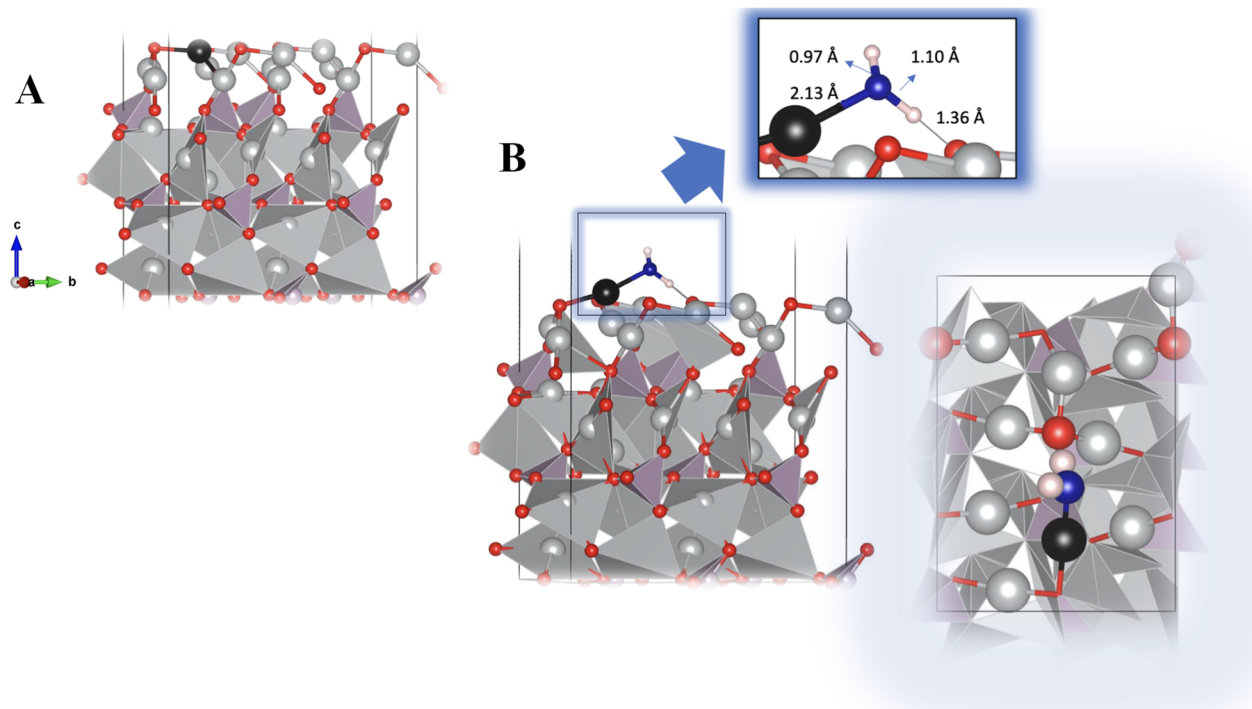


**Figure 5.** (A) Side views of the relaxed clean AP (110) surface. The Ag cation where H<sub>2</sub>O and O<sub>2</sub> molecules adsorb is highlighted in black color. (B) Side and top views of the H<sub>2</sub>O adsorption system. O, P, and Ag atoms on the surface are represented by red, violet, and gray balls, respectively. For clarity, the O and H atoms of the H<sub>2</sub>O molecule are indicated in blue and white colors, respectively.

work, a AP/PP composite was developed and optimized for the first time. This composite has the physicochemical property of oxidizing bacteria (*S. aureus* and *E. coli*), fungi (*C. albicans*), and SARS-COV-2 viruses by surface contact. The adsorption processes of H<sub>2</sub>O and O<sub>2</sub> molecules on the most

active AP (110) surface were modeled through ab initio calculations to explain the early events of the formation of both the hydroxyl radical  $\cdot\text{OH}$  and superoxide radical anion  $\cdot\text{O}_2^-$  as reactive species in the biocide activity.

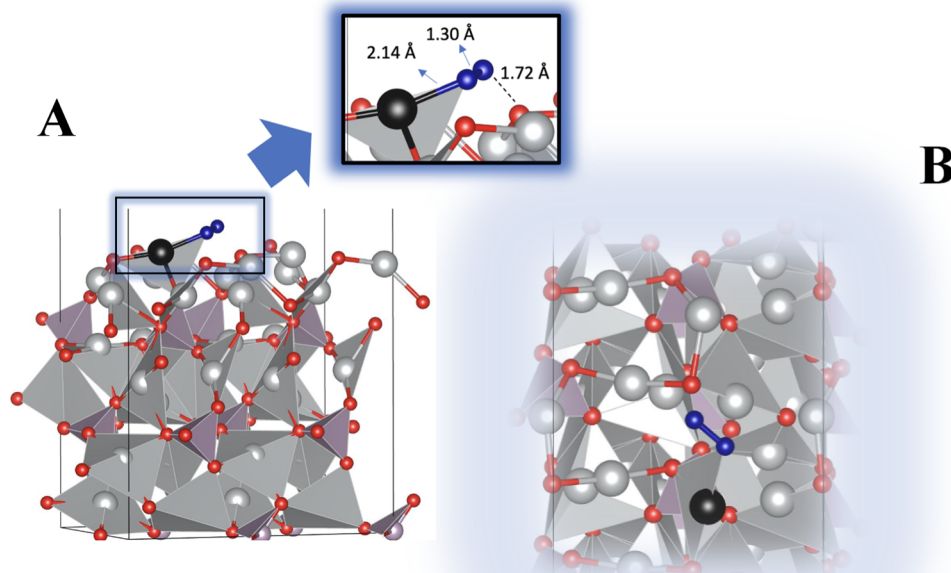


**Figure 6.** Side (A) and top (B) views of one  $O_2$  molecule adsorbed on the AP (110) surface. O, P, and Ag atoms on the surface are represented by red, violet, and gray balls, respectively. For clarity, the Ag adsorption site and the  $O_2$  molecule are colored in black and blue, respectively.

## ■ ASSOCIATED CONTENT

### SI Supporting Information

The Supporting Information is available free of charge at <https://pubs.acs.org/doi/10.1021/acs.jpbc.1c05225>.

Video of the AIMD simulations of the activation of a water molecule on the AP (110) surface at 10 K during 900 fs (MPG)

Detailed experimental and theoretical procedures, structure analyses, DRX, micro-Raman, FTIR, DRS, and AFM, and halo of inhibition tests (PDF) (PDF)

Video of the AIMD simulations of the activation of a water molecule on the AP (110) surface at 50 K during 900 fs (MPG)

## ■ AUTHOR INFORMATION

### Corresponding Author

**Marcelo Assis** – CDMF, LIEC, Federal University of São Carlos—(UFSCar), São Carlos, São Paulo 13565-905, Brazil; Department of Physical and Analytical Chemistry, University Jaume I (UJI), Castelló 12071, Spain; [orcid.org/0000-0003-0355-5565](https://orcid.org/0000-0003-0355-5565); Email: [marcelostassis@gmail.com](mailto:marcelostassis@gmail.com)

### Authors

**Lara K. Ribeiro** – CDMF, LIEC, Federal University of São Carlos—(UFSCar), São Carlos, São Paulo 13565-905, Brazil

**Lais R. Lima** – Chemistry Department, Federal University of São Carlos (UFSCar), São Carlos, São Paulo 13565-905, Brazil; [orcid.org/0000-0002-2159-6320](https://orcid.org/0000-0002-2159-6320)

**Dyovani Coelho** – CDMF, LIEC, Federal University of São Carlos—(UFSCar), São Carlos, São Paulo 13565-905, Brazil; [orcid.org/0000-0002-1652-7144](https://orcid.org/0000-0002-1652-7144)

**Mariana O. Gonçalves** – Biomolecules and Microbiology Laboratory (LaMiB), Biotechnology Graduation Program, Federal University of São Carlos (UFSCar), São Carlos, São Paulo 13565-905, Brazil

**Robert S. Paiva** – Chemistry Department, Federal University of São Carlos (UFSCar), São Carlos, São Paulo 13565-905, Brazil

**Leonardo N. Moraes** – School of Agriculture, São Paulo State University (Unesp), Botucatu, São Paulo 18610-034, Brazil; Molecular Laboratory of Clinical Hospital of Botucatu, Medical School, São Paulo State University (Unesp), Botucatu, São Paulo 18618-687, Brazil

**Lauana F. Almeida** – School of Agriculture, São Paulo State University (Unesp), Botucatu, São Paulo 18610-034, Brazil; Molecular Laboratory of Clinical Hospital of Botucatu, Medical School, São Paulo State University (Unesp), Botucatu, São Paulo 18618-687, Brazil

**Felipe Lipsky** – Institute of Chemistry, State University of Campinas (Unicamp), Campinas, São Paulo 13083-970, Brazil

**Miguel A. San-Miguel** – Institute of Chemistry, State University of Campinas (Unicamp), Campinas, São Paulo 13083-970, Brazil; [orcid.org/0000-0002-6650-7432](https://orcid.org/0000-0002-6650-7432)

**Lúcia H. Mascaro** – CDMF, LIEC, Federal University of São Carlos—(UFSCar), São Carlos, São Paulo 13565-905, Brazil; [orcid.org/0000-0001-6908-1097](https://orcid.org/0000-0001-6908-1097)

**Rejane M. T. Grotto** – School of Agriculture, São Paulo State University (Unesp), Botucatu, São Paulo 18610-034, Brazil; Molecular Laboratory of Clinical Hospital of Botucatu, Medical School, São Paulo State University (Unesp), Botucatu, São Paulo 18618-687, Brazil

**Cristina P. Sousa** – Biomolecules and Microbiology Laboratory (LaMiB), Biotechnology Graduation Program, Federal University of São Carlos (UFSCar), São Carlos, São Paulo 13565-905, Brazil

Ieda L. V. Rosa – CDMF, LIEC, Federal University of São Carlos—(UFSCar), São Carlos, São Paulo 13565-905, Brazil

Sandra A. Cruz – Chemistry Department, Federal University of São Carlos (UFSCar), São Carlos, São Paulo 13565-905, Brazil

Juan Andrés – Department of Physical and Analytical Chemistry, University Jaume I (UJI), Castelló 12071, Spain; [orcid.org/0000-0003-0232-3957](https://orcid.org/0000-0003-0232-3957)

Elson Longo – CDMF, LIEC, Federal University of São Carlos—(UFSCar), São Carlos, São Paulo 13565-905, Brazil; [orcid.org/0000-0001-8062-7791](https://orcid.org/0000-0001-8062-7791)

Complete contact information is available at: <https://pubs.acs.org/10.1021/acs.jpcc.1c05225>

### Author Contributions

L.K.R. and M.A.: Data curation, formal analysis, investigation, methodology, writing—original draft, writing—review and editing, and visualization. L.R.L., D.C., R.S.P., F.L., M.O.G., L.N.M., and L.F.A.: Data curation, formal analysis, methodology, writing—original draft, writing—review and editing, and visualization. L.H.M., R.M.T.G., M.A.S.-M., C.P.S., I.L.V.R., S.A.C., J.A., and E.L.: Funding acquisition, resources, supervision, writing—original draft, writing—review and editing, and visualization.

### Notes

The authors declare no competing financial interest.

### ACKNOWLEDGMENTS

This work was funded in part by Fundação de Amparo à Pesquisa do Estado de São Paulo—FAPESP (2013/07296-2, 2016/13423-5, 2016/23891-6, 2017/26105-4, FAPESP/SHELL 2017/11986-5, 2017/07711-0), Financiadora de Estudos e Projetos—FINEP, Conselho Nacional de Desenvolvimento Científico e Tecnológico—CNPq (166281/2017-4 and 305792/2020-2), and Coordenação de Aperfeiçoamento de Pessoal de Nível Superior—CAPES (finance code 001). J.A. acknowledges Universitat Jaume I (project UJI-B2019-30) and the Ministerio de Ciencia, Innovación y Universidades (Spain) (project PGC2018094417-B-I00) for financially supporting this research. This work used computational resources of the “Centro Nacional de Processamento de Alto Desempenho em São Paulo” (CENAPAD-SP) and “Centro de Computação John David Rogers” (CCJDR-UNICAMP).

### ABBREVIATIONS

AP	silver phosphate, Ag <sub>3</sub> PO <sub>4</sub>
PP	Polypropylene
XRD	X-ray diffraction
FTIR	Fourier transform infrared spectroscopy
AFM	atomic force microscopy
UV–vis	ultraviolet–visible
SEM	scanning electron microscopy
SARS	severe acute respiratory syndrome
MERS	Middle East respiratory syndrome
DFT	density functional theory
ICSD	Inorganic Crystal Structure Database
G′	storage modulus
G″	loss modulus
e <sup>−</sup>	electron
h <sup>+</sup>	hole
E <sub>g</sub>	band gap energy

CFU colony-forming unit

### REFERENCES

- (1) Han, Q.; Lin, Q.; Jin, S.; You, L. Coronavirus 2019-NCov: A Brief Perspective from the Front Line. *J. Infect.* **2020**, *80*, 373–377.
- (2) Guan, W.-j.; Ni, Z.-y.; Hu, Y.; Liang, W.-h.; Ou, C.-q.; He, J.-x.; Liu, L.; Shan, H.; Lei, C.-l.; Hui, D. S. C.; et al. Clinical Characteristics of Coronavirus Disease 2019 in China. *N. Engl. J. Med.* **2020**, *382*, 1708–1720.
- (3) Rothan, H. A.; Byrareddy, S. N. The Epidemiology and Pathogenesis of Coronavirus Disease (COVID-19) Outbreak. *J. Autoimmun.* **2020**, *109*, 102433.
- (4) Chan, J. F.-W.; Kok, K.-H.; Zhu, Z.; Chu, H.; To, K. K.-W.; Yuan, S.; Yuen, K.-Y. Genomic Characterization of the 2019 Novel Human-Pathogenic Coronavirus Isolated from a Patient with Atypical Pneumonia after Visiting Wuhan. *Emerging Microbes Infect.* **2020**, *9*, 221–236.
- (5) Okba, N. M. A.; Müller, M. A.; Li, W.; Wang, C.; GeurtsvanKessel, C. H.; Corman, V. M.; Lamers, M. M.; Sikkema, R. S.; de Bruin, E.; Chandler, F. D.; et al. Severe Acute Respiratory Syndrome Coronavirus 2–Specific Antibody Responses in Coronavirus Disease Patients. *Emerging Infect. Dis.* **2020**, *26*, 1478–1488.
- (6) Su, S.; Wong, G.; Shi, W.; Liu, J.; Lai, A. C. K.; Zhou, J.; Liu, W.; Bi, Y.; Gao, G. F. Epidemiology, Genetic Recombination, and Pathogenesis of Coronaviruses. *Trends Microbiol.* **2016**, *24*, 490–502.
- (7) Shi, J.; Wen, Z.; Zhong, G.; Yang, H.; Wang, C.; Huang, B.; Liu, R.; He, X.; Shuai, L.; Sun, Z.; et al. Susceptibility of Ferrets, Cats, Dogs, and Other Domesticated Animals to SARS-Coronavirus 2. *Science* **2020**, *368*, 1016–1020.
- (8) Li, G.; Fan, Y.; Lai, Y.; Han, T.; Li, Z.; Zhou, P.; Pan, P.; Wang, W.; Hu, D.; Liu, X.; et al. Coronavirus Infections and Immune Responses. *J. Med. Virol.* **2020**, *92*, 424–432.
- (9) Aw, J. The Non-Contact Handheld Cutaneous Infra-Red Thermometer for Fever Screening during the COVID-19 Global Emergency. *J. Hosp. Infect.* **2020**, *104*, 451.
- (10) Chen, H.; Guo, J.; Wang, C.; Luo, F.; Yu, X.; Zhang, W.; Li, J.; Zhao, D.; Xu, D.; Gong, Q.; et al. Clinical Characteristics and Intrauterine Vertical Transmission Potential of COVID-19 Infection in Nine Pregnant Women: A Retrospective Review of Medical Records. *Lancet* **2020**, *395*, 809–815.
- (11) Shereen, M. A.; Khan, S.; Kazmi, A.; Bashir, N.; Siddique, R. COVID-19 infection: Emergence, transmission, and characteristics of human coronaviruses. *J. Adv. Res.* **2020**, *24*, 91–98.
- (12) Qiu, L.; Liu, X.; Xiao, M.; Xie, J.; Cao, W.; Liu, Z.; Morse, A.; Xie, Y.; Li, T.; Zhu, L. SARS-CoV-2 Is Not Detectable in the Vaginal Fluid of Women with Severe COVID-19 Infection. *Clin. Infect. Dis.* **2020**, *71*, 813–817.
- (13) Seminara, G.; Carli, B.; Forni, G.; Fuzzi, S.; Mazzino, A.; Rinaldo, A. Biological Fluid Dynamics of Airborne COVID-19 Infection. *Rend. Lincei* **2020**, *31*, 505–537.
- (14) Razzini, K.; Castrica, M.; Menchetti, L.; Maggi, L.; Negroni, L.; Orfeo, N. V.; Pizzoccheri, A.; Stocco, M.; Muttini, S.; Balzaretto, C. M. SARS-CoV-2 RNA detection in the air and on surfaces in the COVID-19 ward of a hospital in Milan, Italy. *Sci. Total Environ.* **2020**, *742*, 140540.
- (15) Wu, S.; Wang, Y.; Jin, X.; Tian, J.; Liu, J.; Mao, Y. Environmental Contamination by SARS-CoV-2 in a Designated Hospital for Coronavirus Disease 2019. *Am. J. Infect. Control* **2020**, *48*, 910–914.
- (16) Vardoulakis, S.; Sheel, M.; Lal, A.; Gray, D. COVID-19 environmental transmission and preventive public health measures. *Aust. N. Z. J. Public Health* **2020**, *44*, 333–335.
- (17) Tremiliosi, G. C.; Simoes, L. G. P.; Minozzi, D. T.; Santos, R. I.; Vilela, D. C. B.; Durigon, E. L.; Machado, R. R. G.; Medina, D. S.; Ribeiro, L. K.; Rosa, I. L. V.; et al. Ag Nanoparticles-Based Antimicrobial Polycotton Fabrics to Prevent the Transmission and Spread of SARS-CoV-2. *bioRxiv*: 2020.06.26.152520, **2020**.

- (18) Gupta, A.; Mumtaz, S.; Li, C.-H.; Hussain, I.; Rotello, V. M. Combatting Antibiotic-Resistant Bacteria Using Nanomaterials. *Chem. Soc. Rev.* **2019**, *48*, 415–427.
- (19) Assis, M.; de Foggi, C. C.; Teodoro, V.; de Campos da Costa, J. P.; Silva, C. E.; Robeldo, T.; Caperucci, P. F.; Vergani, C. E.; Borra, R. C.; Sorribes, I.; et al. Surface-Dependent Photocatalytic and Biological Activities of  $\text{Ag}_2\text{CrO}_4$ : Integration of Experiment and Simulation. *Appl. Surf. Sci.* **2021**, *545*, 148964.
- (20) Pinatti, I. M.; Tello, A. C. M.; Trench, A. B.; de Foggi, C. C.; Pereira, P. F. S.; Teixeira, M. M.; Jacomaci, N.; Andrés, J.; Longo, E. Zinc-Substituted  $\text{Ag}_2\text{CrO}_4$ : A Material with Enhanced Photocatalytic and Biological Activity. *J. Alloys Compd.* **2020**, *835*, 155315.
- (21) Alvarez-Roca, R.; Gouveia, A. F.; de Foggi, C. C.; Lemos, P. S.; Gracia, L.; da Silva, L. F.; Vergani, C. E.; San-Miguel, M.; Longo, E.; Andrés, J. Selective Synthesis of  $\alpha$ -,  $\beta$ -, and  $\gamma$ - $\text{Ag}_2\text{WO}_4$  Polymorphs: Promising Platforms for Photocatalytic and Antibacterial Materials. *Inorg. Chem.* **2021**, *60*, 1062–1079.
- (22) Foggi, C. C.; Fabbro, M. T.; Santos, L. P. S.; de Santana, Y. V. B.; Machado, A. L.; Cordoncillo, E.; Andrés, J.; Longo, E.; Longo, E. Synthesis and Evaluation of  $\alpha$ - $\text{Ag}_2\text{WO}_4$  as Novel Antifungal Agent. *Chem. Phys. Lett.* **2017**, *674*, 125–129.
- (23) Cruz-Filho, J. F.; Costa, T. M. S.; Lima, M. S.; Nolêto, L. F. G.; Bandeira, C. C. S.; Lima, F. L.; Luz, G. E. Microorganisms Photocatalytic Inactivation on  $\text{Ag}_3\text{PO}_4$  Sub-Microcrystals Under WLEDs Light Source. *J. Inorg. Organomet. Polym. Mater.* **2021**, *31*, 2233.
- (24) de Foggi, C. C.; de Oliveira, R. C.; Fabbro, M. T.; Vergani, C. E.; Andres, J.; Longo, E.; Machado, A. L. Tuning the Morphological, Optical, and Antimicrobial Properties of  $\alpha$ - $\text{Ag}_2\text{WO}_4$  Microcrystals Using Different Solvents. *Cryst. Growth Des.* **2017**, *17*, 6239–6246.
- (25) de Oliveira, R. C.; de Foggi, C. C.; Teixeira, M. M.; da Silva, M. D. P.; Assis, M.; Francisco, E. M.; Pimentel, B. N. A. d. S.; Pereira, P. F. d. S.; Vergani, C. E.; Machado, A. L.; et al. Mechanism of Antibacterial Activity via Morphology Change of  $\alpha$ - $\text{AgVO}_3$ : Theoretical and Experimental Insights. *ACS Appl. Mater. Interfaces* **2017**, *9*, 11472–11481.
- (26) De Foggi, C. C.; De Oliveira, R. C.; Assis, M.; Fabbro, M. T.; Mastelaro, V. R.; Vergani, C. E.; Gracia, L.; Andrés, J.; Longo, E.; Machado, A. L. Unveiling the Role of  $\beta$ - $\text{Ag}_2\text{MoO}_4$  Microcrystals to the Improvement of Antibacterial Activity. *Mater. Sci. Eng., C* **2020**, *111*, 110765.
- (27) Gouveia, A. F.; Gracia, L.; Longo, E.; San-Miguel, M. A.; Andrés, J. Modulating the Properties of Multifunctional Semiconductors by Means of Morphology: Theory Meets Experiments. *Comput. Mater. Sci.* **2021**, *188*, 110217.
- (28) Yi, Z.; Ye, J.; Kikugawa, N.; Kako, T.; Ouyang, S.; Stuart-Williams, H.; Yang, H.; Cao, J.; Luo, W.; Li, Z.; et al. An Orthophosphate Semiconductor with Photooxidation Properties under Visible-Light Irradiation. *Nat. Mater.* **2010**, *9*, 559–564.
- (29) Zhang, H.; Huang, H.; Ming, H.; Li, H.; Zhang, L.; Liu, Y.; Kang, Z. Carbon Quantum Dots/ $\text{Ag}_3\text{PO}_4$  Complex Photocatalysts with Enhanced Photocatalytic Activity and Stability under Visible Light. *J. Mater. Chem.* **2012**, *22*, 10501–10506.
- (30) Botelho, G.; Andres, J.; Gracia, L.; Matos, L. S.; Longo, E. Photoluminescence and Photocatalytic Properties of  $\text{Ag}_3\text{PO}_4$  Microcrystals: An Experimental and Theoretical Investigation. *Chempluschem* **2016**, *81*, 202–212.
- (31) Trench, A. B.; Machado, T. R.; Gouveia, A. F.; Foggi, C. C.; Teodoro, V.; Sánchez-Montes, I.; Teixeira, M. M.; Da Trindade, L. G.; Jacomaci, N.; Perrin, A.; et al. Rational Design of W-Doped  $\text{Ag}_3\text{PO}_4$  as an Efficient Antibacterial Agent and Photocatalyst for Organic Pollutant Degradation. *ACS Omega* **2020**, *5*, 23808–23821.
- (32) Rakibuddin, M.; Ananthakrishnan, R. A Novel Ag Deposited Nanocoordination Polymer Derived Porous  $\text{SnO}_2/\text{NiO}$  Heteronanostructure for the Enhanced Photocatalytic Reduction of Cr(VI) under Visible Light. *New J. Chem.* **2016**, *40*, 3385–3394.
- (33) Dinh, C.-T.; Nguyen, T.-D.; Kleitz, F.; Do, T.-O. Large-Scale Synthesis of Uniform Silver Orthophosphate Colloidal Nanocrystals Exhibiting High Visible Light Photocatalytic Activity. *Chem. Commun.* **2011**, *47*, 7797–7799.
- (34) Huang, K.; Lv, Y.; Zhang, W.; Sun, S.; Yang, B.; Chi, F.; Ran, S.; Liu, X. One-Step Synthesis of  $\text{Ag}_3\text{PO}_4/\text{Ag}$  Photocatalyst with Visible-Light Photocatalytic Activity. *Mater. Res.* **2015**, *18*, 939–945.
- (35) Costa, T. M. S.; Lima, M. S.; Cruz Filho, J. F.; Silva, L. J.; Santos, R. S.; Luz, G. E. Synthesis, Characterization, and Photocatalytic Activity of  $\text{Ag}_3\text{PO}_4/\text{SBA-15}$  in Ciprofloxacin Degradation under Polychromatic Irradiation. *J. Photochem. Photobiol., A* **2018**, *364*, 461–471.
- (36) Cruz-Filho, J. F.; Costa, T. M. S.; Lima, M. S.; Silva, L. J.; Santos, R. S.; Cavalcante, L. S.; Longo, E.; Luz, G. E. Effect of Different Synthesis Methods on the Morphology, Optical Behavior, and Superior Photocatalytic Performances of  $\text{Ag}_3\text{PO}_4$  Sub-Microcrystals Using White-Light-Emitting Diodes. *J. Photochem. Photobiol., A* **2019**, *377*, 14–25.
- (37) de Costa, J. P. C.; Assis, M.; Teodoro, V.; Rodrigues, A.; Cristina de Foggi, C.; San-Miguel, M. A.; Pereira do Carmo, J. P.; Andrés, J.; Longo, E. Electron Beam Irradiation for the Formation of Thick Ag Film on  $\text{Ag}_3\text{PO}_4$ . *RSC Adv.* **2020**, *10*, 21745–21753.
- (38) dos Santos, C. C.; Assis, M.; Machado, T. R.; dos Santos Pereira, P. F.; Minguez-Vega, G.; Cordoncillo, E.; Beltran-Mir, H.; Doñate-Buendía, C.; Andrés, J.; Longo, E. Proof-of-Concept Studies Directed toward the Formation of Metallic Ag Nanostructures from  $\text{Ag}_3\text{PO}_4$  Induced by Electron Beam and Femtosecond Laser. *Part. Part. Syst. Charact.* **2019**, *36*, 1800533.
- (39) Botelho, G.; Szczancoski, J. C.; Andres, J.; Gracia, L.; Longo, E. Experimental and Theoretical Study on the Structure, Optical Properties, and Growth of Metallic Silver Nanostructures in  $\text{Ag}_3\text{PO}_4$ . *J. Phys. Chem. C* **2015**, *119*, 6293–6306.
- (40) Guo, R.; Wu, J.; Xu, A.; Huang, X.; Zhu, H.; Jiang, R.; Lin, Y.; Guo, F.  $\text{ZnWO}_4/\text{Ag}_3\text{PO}_4$  Composites with an Enhanced Photocatalytic Activity and Stability under Visible Light. *RSC Adv.* **2016**, *6*, 114818–114824.
- (41) Hsieh, M.-S.; Su, H.-J.; Hsieh, P.-L.; Chiang, Y.-W.; Huang, M. H. Synthesis of  $\text{Ag}_3\text{PO}_4$  Crystals with Tunable Shapes for Facet-Dependent Optical Property, Photocatalytic Activity, and Electrical Conductivity Examinations. *ACS Appl. Mater. Interfaces* **2017**, *9*, 39086–39093.
- (42) Li, X.; Xu, P.; Chen, M.; Zeng, G.; Wang, D.; Chen, F.; Tang, W.; Chen, C.; Zhang, C.; Tan, X. Application of Silver Phosphate-Based Photocatalysts: Barriers and Solutions. *Chem. Eng. J.* **2019**, *366*, 339–357.
- (43) Kamal, M. M.; Safan, M. A.; Etman, Z. A.; Kasem, B. M. Mechanical Properties of Self-Compacted Fiber Concrete Mixes. *HBRC J.* **2014**, *10*, 25–34.
- (44) Ghaffari, M.; Mollazadeh-Bajestani, M.; Moztaarzadeh, F.; Uludağ, H.; Hardy, J. G.; Mozafari, M. An Overview of the Use of Biomaterials, Nanotechnology, and Stem Cells for Detection and Treatment of COVID-19: Towards a Framework to Address Future Global Pandemics. *Emergent Mater.* **2021**, *4*, 19–34.
- (45) Martí, M.; Tuñón-Molina, A.; Aachmann, F.; Muramoto, Y.; Noda, T.; Takayama, K.; Serrano-Aroca, A. Protective Face Mask Filter Capable of Inactivating SARS-CoV-2, and Methicillin-Resistant Staphylococcus Aureus and Staphylococcus Epidermidis. *Polymers* **2021**, *13*, 207.
- (46) Abraham, J.; Sharika, T.; George, S. C.; Thomas, S. Rheology: Open Access Rheological Percolation in Thermoplastic Polymer Nanocomposites. *Rheol. Open access* **2017**, *1*, 1–15.
- (47) Terpilowski, K.; Rymuszka, D.; Holysz, L.; Chibowski, E. Changes in Wettability of Polycarbonate and Polypropylene Pre-treated With Oxygen and Argon Plasma. *Proceedings of the 8th International Conference MMT-20142, Ariel, Israel, 2014; Vol. 4*, pp 155–165.
- (48) Kasraei, S.; Azarsina, M. Addition of Silver Nanoparticles Reduces the Wettability of Methacrylate and Silorane-Based Composites. *Braz. Oral Res.* **2012**, *26*, 505–510.
- (49) Liu, Q.; Brookbank, L.; Ho, A.; Coffey, J.; Brennan, A. B.; Jones, C. J. Surface Texture Limits Transfer of S. Aureus, T4



Bacteriophage, Influenza B Virus and Human Coronavirus. *PLoS One* **2021**, *15*, No. e0244518.

(50) Hosseini, M.; Chin, A. W. H.; Behzadinasab, S.; Poon, L. L. M.; Ducker, W. A. Cupric Oxide Coating That Rapidly Reduces Infection by SARS-CoV-2 via Solids. *ACS Appl. Mater. Interfaces* **2021**, *13*, 5919.

(51) Piccirillo, C.; Pinto, R. A.; Tobaldi, D. M.; Pullar, R. C.; Labrincha, J. A.; Pintado, M. M. E.; Castro, P. M. L. Light Induced Antibacterial Activity and Photocatalytic Properties of Ag<sub>3</sub>PO<sub>4</sub>-Based Material of Marine Origin. *J. Photochem. Photobiol., A* **2015**, *296*, 40–47.

(52) Gherasim, O.; Puiu, R. A.; Bircă, A. C.; Burdușel, A.-C.; Grumezescu, A. M. An Updated Review on Silver Nanoparticles in Biomedicine. *Nanomaterials* **2020**, *10*, 2318–44.

(53) Liou, J.-W.; Chang, H.-H. Bactericidal Effects and Mechanisms of Visible Light-Responsive Titanium Dioxide Photocatalysts on Pathogenic Bacteria. *Arch. Immunol. Ther. Exp* **2012**, *60*, 267–275.

(54) Macedo, N. G.; Machado, T. R.; Roca, R. A.; Assis, M.; Foggi, C. C.; Puerto-Belda, V.; Mínguez-Vega, G.; Rodrigues, A.; San-Miguel, M. A.; Cordoncillo, E.; et al. Tailoring the Bactericidal Activity of Ag Nanoparticles/ $\alpha$ -Ag<sub>2</sub>WO<sub>4</sub> Composite Induced by Electron Beam and Femtosecond Laser Irradiation: Integration of Experiment and Computational Modeling. *ACS Appl. Bio Mater.* **2019**, *2*, 824–837.

(55) Roca, R. A.; Sczancoski, J. C.; Nogueira, I. C.; Fabbro, M. T.; Alves, H. C.; Gracia, L.; Santos, L. P. S.; De Sousa, C. P.; Andrés, J.; Luz, G. E.; et al. Facet-Dependent Photocatalytic and Antibacterial Properties of  $\alpha$ -Ag<sub>2</sub>WO<sub>4</sub> Crystals: Combining Experimental Data and Theoretical Insights. *Catal. Sci. Technol.* **2015**, *5*, 4091–4107.

(56) Abram, S. L.; Fromm, K. M. Handling (Nano)Silver as Antimicrobial Agent: Therapeutic Window, Dissolution Dynamics, Detection Methods and Molecular Interactions. *Chem.—Eur. J.* **2020**, *26*, 10948–10971.

(57) Choi, Y.; Kim, H.-A.; Kim, K.-W.; Lee, B.-T. Comparative Toxicity of Silver Nanoparticles and Silver Ions to Escherichia Coli. *J. Environ. Sci.* **2018**, *66*, 50–60.

(58) Berlanga, M.; Montero, M. T.; Hernández-Borrell, J.; Viñas, M. Influence of the Cell Wall on Ciprofloxacin Susceptibility in Selected Wild-Type Gram-Negative and Gram-Positive Bacteria. *Int. J. Antimicrob. Agents* **2004**, *23*, 627–630.

(59) Barzegar, H.; Zahed, M. A.; Vatanpour, V. Antibacterial and Antifouling Properties of Ag<sub>3</sub>PO<sub>4</sub>/GO Nanocomposite Blended Polyethersulfone Membrane Applied in Dye Separation. *J. Water Process Eng.* **2020**, *38*, 101638.

(60) Tamiyakul, H.; Roytrakul, S.; Jaresitthikunchai, J.; Phaonakrop, N.; Tanasupawat, S.; Warisnoicharoen, W. Changes in Protein Patterns of Staphylococcus Aureus and Escherichia Coli by Silver Nanoparticles Capped with Poly (4-Styrenesulfonic Acid-Co-Maleic Acid) Polymer. *Asian Biomed.* **2019**, *13*, 39–47.

(61) Salleh, A.; Naomi, R.; Utami, N. D.; Mohammad, A. W.; Mahmoudi, E.; Mustafa, N.; Fauzi, M. B. The Potential of Silver Nanoparticles for Antiviral and Antibacterial Applications: A Mechanism of Action. *Nanomaterials* **2020**, *10*, 1566.

(62) Nakamura, S.; Sato, M.; Sato, Y.; Ando, N.; Takayama, T.; Fujita, M.; Ishihara, M. Synthesis and Application of Silver Nanoparticles (Ag NPs) for the Prevention of Infection in Healthcare Workers. *Int. J. Mol. Sci.* **2019**, *20*, 3620.

(63) Kubo, A.-L.; Capijak, I.; Vrček, I. V.; Bondarenko, O. M.; Kurvet, I.; Vija, H.; Ivask, A.; Kasemets, K.; Kahru, A. Antimicrobial Potency of Differently Coated 10 and 50 Nm Silver Nanoparticles against Clinically Relevant Bacteria Escherichia Coli and Staphylococcus Aureus. *Colloids Surf., B* **2018**, *170*, 401–410.

(64) Chang, B.-M.; Pan, L.; Lin, H.-H.; Chang, H.-C. Nano-diamond-Supported Silver Nanoparticles as Potent and Safe Antibacterial Agents. *Sci. Rep.* **2019**, *9*, 1–11.

(65) Basak, S.; Packirisamy, G. Nano-Based Antiviral Coatings to Combat Viral Infections. *Nano-Struct. Nano-Objects* **2020**, *24*, 100620.

(66) Mukherjee, S.; Mazumder, P.; Joshi, M.; Joshi, C.; Dalvi, S. V.; Kumar, M. Biomedical Application, Drug Delivery and Metabolic

Pathway of Antiviral Nanotherapeutics for Combating Viral Pandemic: A Review. *Environ. Res.* **2020**, *191*, 110119.

(67) Jeremiah, S. S.; Miyakawa, K.; Morita, T.; Yamaoka, Y.; Ryo, A. Potent Antiviral Effect of Silver Nanoparticles on SARS-CoV-2. *Biochem. Biophys. Res. Commun.* **2020**, *533*, 195–200.

(68) Assis, M.; Simoes, L. G. P.; Tremiliosi, G. C.; Coelho, D.; Minozzi, D. T.; Santos, R. I.; Vilela, D. C. B.; Santos, J. R. d.; Ribeiro, L. K.; Rosa, I. L. V.; et al. SiO<sub>2</sub>-Ag Composite as a Highly Virucidal Material: A Roadmap That Rapidly Eliminates SARS-CoV-2. *Nanomaterials* **2021**, *11*, 638.

(69) Lakshmi Prasanna, V.; Vijayaraghavan, R. Insight into the Mechanism of Antibacterial Activity of ZnO: Surface Defects Mediated Reactive Oxygen Species Even in the Dark. *Langmuir* **2015**, *31*, 9155–9162.

(70) Zhang, W.; Li, Y.; Niu, J.; Chen, Y. Photogeneration of Reactive Oxygen Species on Uncoated Silver, Gold, Nickel, and Silicon Nanoparticles and Their Antibacterial Effects. *Langmuir* **2013**, *29*, 4647–4651.

(71) Li, Y.; Zhang, W.; Niu, J.; Chen, Y. Mechanism of Photogenerated Reactive Oxygen Species and Correlation with the Antibacterial Properties of Engineered Metal-Oxide Nanoparticles. *ACS Nano* **2012**, *6*, 5164–5173.

(72) Fujii, M.; Usui, M.; Hayashi, S.; Gross, E.; Kovalev, D.; Künzner, N.; Diener, J.; Timoshenko, V. Y. Chemical reaction mediated by excited states of Si nanocrystals-Singlet oxygen formation in solution. *J. Appl. Phys.* **2004**, *95*, 3689–3693.

(73) Du, J.; Gebicki, J. M. Proteins Are Major Initial Cell Targets of Hydroxyl Free Radicals. *Int. J. Biochem. Cell Biol.* **2004**, *36*, 2334–2343.

(74) Tian, Z.; Li, X.; Ma, Y.; Chen, T.; Xu, D.; Wang, B.; Qu, Y.; Gao, Y. Quantitatively Intrinsic Biomimetic Catalytic Activity of Nanocerias as Radical Scavengers and Their Ability against H<sub>2</sub>O<sub>2</sub> and Doxorubicin-Induced Oxidative Stress. *ACS Appl. Mater. Interfaces* **2017**, *9*, 23342–23352.

(75) Guo, R.; Fan, Y.; Tang, Y. Interesting Ag<sub>3</sub>PO<sub>4</sub> Concave Rhombic Dodecahedra: The Same Face with Different Morphologies and Photocatalytic Properties. *RSC Adv.* **2017**, *7*, 23977–23981.

(76) Wang, H.; He, L.; Wang, L.; Hu, P.; Guo, L.; Han, X.; Li, J. Facile Synthesis of Ag<sub>3</sub>PO<sub>4</sub> Tetrapod Microcrystals with an Increased Percentage of Exposed {110} Facets and Highly Efficient Photocatalytic Properties. *CrystEngComm* **2012**, *14*, 8342–8344.

(77) Wang, J.; Teng, F.; Chen, M.; Xu, J.; Song, Y.; Zhou, X. Facile Synthesis of Novel Ag<sub>3</sub>PO<sub>4</sub> Tetrapods and the {110} Facets-Dominated Photocatalytic Activity. *CrystEngComm* **2013**, *15*, 39–42.

(78) Li, M.; Chen, M.; Wang, J.; Teng, F. Branching Growth of Novel Silver Phosphate Dendrites and the Greatly Improved Photocatalytic Activity by the Active {110} Facets. *CrystEngComm* **2014**, *16*, 1237–1240.

(79) Batvandi, M.; Haghghatizadeh, A.; Mazinani, B. Synthesis of Ag<sub>3</sub>PO<sub>4</sub> Microstructures with Morphology-Dependent Optical and Photocatalytic Behaviors. *Appl. Phys. A* **2020**, *126*, 571.

(80) Lipsky, F.; Lacerda, L. H. D. S.; De Lazaro, S. R.; Longo, E.; Andrés, J.; San-Miguel, M. A. Unraveling the Relationship between Exposed Surfaces and the Photocatalytic Activity of Ag<sub>3</sub>PO<sub>4</sub>: An in-Depth Theoretical Investigation. *RSC Adv.* **2020**, *10*, 30640–30649.

(81) Bi, Y.; Ouyang, S.; Umezawa, N.; Cao, J.; Ye, J. Facet Effect of Single-Crystalline Ag<sub>3</sub>PO<sub>4</sub> Sub-Microcrystals on Photocatalytic Properties. *J. Am. Chem. Soc.* **2011**, *133*, 6490–6492.

(82) Bomio, M. R. D.; Tranquilin, R. L.; Motta, F. V.; Paskocimas, C. A.; Nascimento, R. M.; Gracia, L.; Andres, J.; Longo, E. Toward Understanding the Photocatalytic Activity of PbMoO<sub>4</sub> Powders with Predominant (111), (100), (011), and (110) Facets. A Combined Experimental and Theoretical Study. *J. Phys. Chem. C* **2013**, *117*, 21382–21395.

(83) Lazzeri, M.; Vittadini, A.; Selloni, A. Structure and Energetics of Stoichiometric TiO<sub>2</sub> Anatase Surfaces. *Phys. Rev. B: Condens. Matter Mater. Phys.* **2001**, *63*, 155409.

(84) Eugen Schwarz, W. H.; Bader, W. H. R. F. Richard F. Bader: Atoms in Molecules (A Quantum Theory) Clarendon Press 1990,

Oxford. ISBN 019-855-1681, 438 pages, Preis: £50.-. *Ber. Bunsengesellschaft für Phys. Chemie* **1991**, 95, 1308.